


Thermomechanical Nanocutting of 2D Materials

Xia Liu, Samuel Tobias Howell, Ana Conde-Rubio, Giovanni Boero, and Juergen Brugger*

Atomically thin materials, such as graphene and transition metal dichalcogenides, are promising candidates for future applications in micro/nanodevices and systems. For most applications, functional nanostructures have to be patterned by lithography. Developing lithography techniques for 2D materials is essential for system integration and wafer-scale manufacturing. Here, a thermomechanical indentation technique is demonstrated, which allows for the direct cutting of 2D materials using a heated scanning nanotip. Arbitrarily shaped cuts with a resolution of 20 nm are obtained in monolayer 2D materials, i.e., molybdenum ditelluride (MoTe_2), molybdenum disulfide (MoS_2), and molybdenum diselenide (MoSe_2), by thermomechanically cleaving the chemical bonds and by rapid sublimation of the polymer layer underneath the 2D material layer. Several micro/nanoribbon structures are fabricated and electrically characterized to demonstrate the process for device fabrication. The proposed direct nanocutting technique allows for precisely tailoring nanostructures of 2D materials with foreseen applications in the fabrication of electronic and photonic nanodevices.

2D materials such as molybdenum disulfide (MoS_2), black phosphorus, and molybdenum ditelluride (MoTe_2) are considered viable key components for diverse nanoelectronics applications. This is mainly due to their atomically thin structures and extraordinary properties beyond bulk counterparts, enabling applications where for instance flexibility and stretchability are important.^[1,2] The increasing diversity of the 2D material family with emerging unique and remarkable properties has led to consider them to be part of the next generation of flexible nanoelectronics and nanophotonics.^[3] The capability of producing high-quality 2D material nanostructures with well-defined geometries at high resolution is a critical requirement for fostering 2D material-based applications. For instance, patterning atomically thin materials into finite structures with nanometer-scale confinement is important for tuning their electronic transport properties^[4] but remains a major challenge. Scaling of electronic devices to smaller dimensions also increases the device density and reduces power consumption.^[5]

Dr. X. Liu, Dr. S. T. Howell, Dr. A. Conde-Rubio, Dr. G. Boero,
 Prof. J. Brugger
 Microsystems Laboratory
 École Polytechnique Fédérale de Lausanne (EPFL)
 Lausanne 1015, Switzerland
 E-mail: juergen.brugger@epfl.ch

 The ORCID identification number(s) for the author(s) of this article can be found under <https://doi.org/10.1002/adma.202001232>.

© 2020 The Authors. Published by WILEY-VCH Verlag GmbH & Co. KGaA, Weinheim. This is an open access article under the terms of the Creative Commons Attribution-NonCommercial License, which permits use, distribution and reproduction in any medium, provided the original work is properly cited and is not used for commercial purposes.

DOI: 10.1002/adma.202001232

To produce nanostructures of 2D materials, top-down techniques such as photolithography,^[6] electron beam lithography (EBL),^[7] and ion beam lithography^[8] are typically used. It has been recently observed that the lithographic techniques using electrons or ions may induce structural damage in 2D materials,^[9] or add resist contaminations that need to be removed by plasma cleaning.^[10] Laser ablation is a resist-free, one-step alternative,^[11–13] but the optical diffraction limit prevents its use where sub-micrometer resolution is required. Bottom-up techniques, like chemical vapor deposition and site-selective growth,^[14,15] allow for scalability and high resolution. However, reproducible fabrication of complex device structures and device integration is still unsolved.

Scanning probe lithography (SPL) embraces a set of nanolithographic techniques that enable unique applications requiring ultrahigh resolution.^[16] The working principle of SPL is based on various physical and chemical interactions between a nanoprobe and the surface and has also been applied to 2D materials for mechanical scratching,^[17] local oxidation,^[18,19] and dip-pen processes.^[5] Specifically, thermal scanning probe lithography (t-SPL) is an emerging direct-write method that uses a heated nanotip for 2D and 3D subtractive/additive manufacturing.^[20–22] The creation of patterns by t-SPL is accomplished by consecutive indentation of the sample with the heated nanotip while simultaneously scanning the sample. In addition to ultrafast writing, the sample can be imaged with the cold tip similar to conventional atomic force microscopy (AFM), enabling closed-loop lithography and pattern overlay. Here we show that the thermomechanical indentation technique that is typically applied to sublimable polymers also allows for the direct cutting of 2D materials. To do so, we use the t-SPL under ambient pressure and temperature to locally thermomechanically cleave the chemical bonds of 2D materials with the heated nanotip. 20 nm resolution patterns of monolayer MoTe_2 are demonstrated, as well as its applicability to other 2D materials, such as MoS_2 and MoSe_2 . With respect to EBL, the proposed technique does not require high vacuum and avoids electron-induced damage, therefore it can readily be implemented in a very cost-effective manner to prototype and fabricate high-quality 2D nanostructures.

For most applications, functional nanostructures of 2D materials have to be patterned by lithography techniques. Here, we developed a one-step lithography technique, also named direct nanocutting, for monolayer 2D materials using a thermomechanical indentation method, as illustrated in **Figure 1a**. To do so, we transferred a 2D material flake directly onto a 50 nm thick sublimable polymer layer that was spin

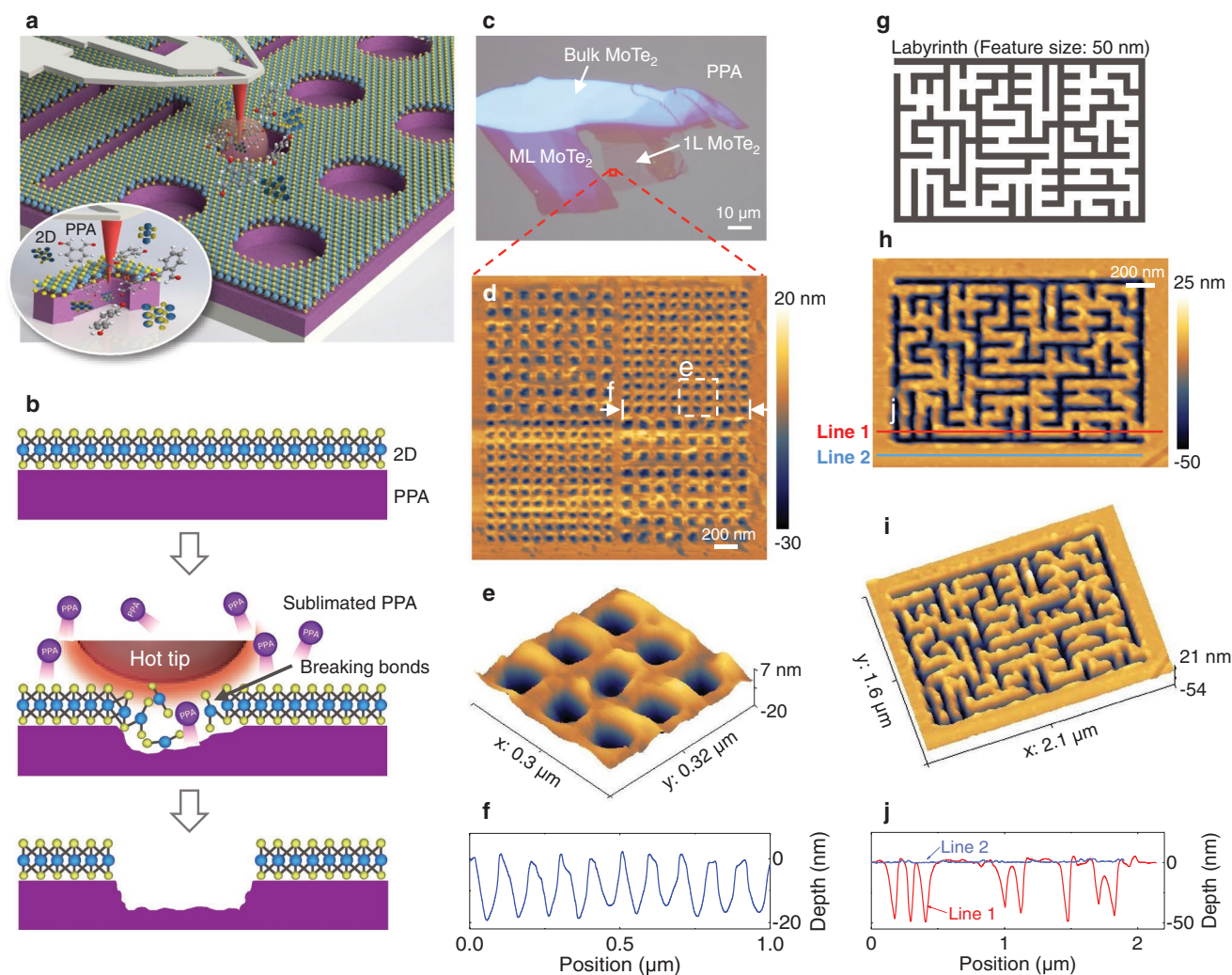


Figure 1. Thermomechanical indentation technique for 2D materials and fabrication results. a) Conceptual schematic of the t-SPL applied to 2D materials which can be cut and locally removed at nanoscale. For clarity, the size of the tip is not to scale. b) Cross-sectional view of 2D material cutting using t-SPL. c) A monolayer/multilayer (1L/ML) MoTe_2 flake is dry transferred on a 50 nm thick PPA layer spin coated on a SiO_2/Si substrate. d) AFM topography of the fabricated MoTe_2 nanosquare structures with 50 nm side (top right and bottom left) and 70 nm (top left and bottom right). e) Magnified 3D topography of the selected area in (d). f) Depth profile of the selected line in (d). The cutting depth is around 20 nm. g) Pattern used to create the 2D material labyrinth. The feature size is 50 nm. h) AFM topography of the MoTe_2 labyrinth nanostructure showing the capability of on-demand cutting. The feature size of the fabricated labyrinth structure is around 55 nm. i) The corresponding 3D topography of (h). j) Depth profiles of the selected cross-sections in (h).

coated on a $\text{SiO}_2/\text{silicon}$ substrate. The cutting is performed by approaching the heated nanotip to the 2D material surface and by applying a sufficiently high force (or pressure) such that the chemical bonds in the 2D layer are broken. The resulting cut exposes the underlying polymer to the heat emitted by the nanotip, which results in sublimation of the polymer and thereby creating a deeper indent (Figure 1b). The sublimation of the polymer in fact facilitates the tip to physically break the chemical bonds. This is very different with respect to earlier work describing the mechanical scratching of 2D material on an inelastic SiO_2 surface using an AFM tip.^[17] The polymer we use is polyphthalaldehyde (PPA) with a glass transition temperature of $\approx 150^\circ\text{C}$. Above this temperature, the PPA polymer chains break and simultaneously unzip into small volatile molecules.^[23] Consequently, PPA does not melt, but directly

sublimates and thus enables the localized depolymerization at sub-10 nm scale and at high speed.^[24] It is currently our understanding that the combination of both the heat and the force is central for the cutting of 2D materials. Indeed, the thermomechanical indentation enables the tip to displace the 2D layer sufficiently deep into the PPA layer until the chemical bonds of the 2D layer break, allowing the PPA to sublime. Thus, the scanning nanotip creates nanocuts in the order of the tip diameter and thereby delineates any required layout in the 2D layer to yield ribbons with variable geometries.

We systematically studied the cutting capability on several 2D materials (MoTe_2 , MoS_2 , MoSe_2 , and graphene), having different number of layers, in particular, monolayer (1L), two layers (2L), and three layers (3L). These 2D materials have breaking strengths ranging from 3 to 42 N m^{-1} .^[25–29] Depending on this

value, the cutting can be performed, or not, at a given writing temperature and indentation force. We first designed a test pattern consisting of nanosquare arrays and a labyrinth pattern in a 1L MoTe₂ flake (Figure 1c). Figure 1d shows nanosquare arrays in the 1L MoTe₂ flake with side lengths of 50 and 70 nm. The number of layers is identified by Raman spectroscopy (Section S1, Supporting Information). The patterning speed of the probe is 0.5 mm s⁻¹ and the total time of writing and imaging spent on the 2.5 × 2.5 μm² area in Figure 1d is 45 s. The 3D topography, as measured by AFM (Dimension FastScan AFM system, Bruker) (Section S2, Supporting Information), shows that the PPA polymer has well-defined 3D nanopatterns (Figure 1e). Figure 1f shows the cross-section profile of the selected area in Figure 1d with nanosquares having an average width of 50 nm and a uniform depth of 20 nm. The indentation depth of these structures corresponds to straining the 2D layer

twice as high as the calculated breaking strength.^[25] Although it is difficult to experimentally determine the strain at which the 2D material breaks, these results clearly show that a cut has been achieved. Nanocutting of continuous lines in 1L MoTe₂ is also successfully conducted in a labyrinth pattern (Figure 1g) with a linewidth of 50 nm as shown in Figure 1h–j.

To investigate the patterning capability at various scales we performed nanocutting experiments to create square patterns that have feature sizes ranging from 20 to 200 nm (Figure 2). The smallest feature we were able to cut is about 20 nm, which is the smallest reported for a direct cutting method and is similar to the resolution in EBL. Our direct nanofabrication technique is not limited to monolayer MoTe₂ but can be also used to cut other 2D materials, certain multilayers and, most interestingly, also heterostructures. To break the 2D layer apart, the indenting tip has to induce sufficient deformation to reach the

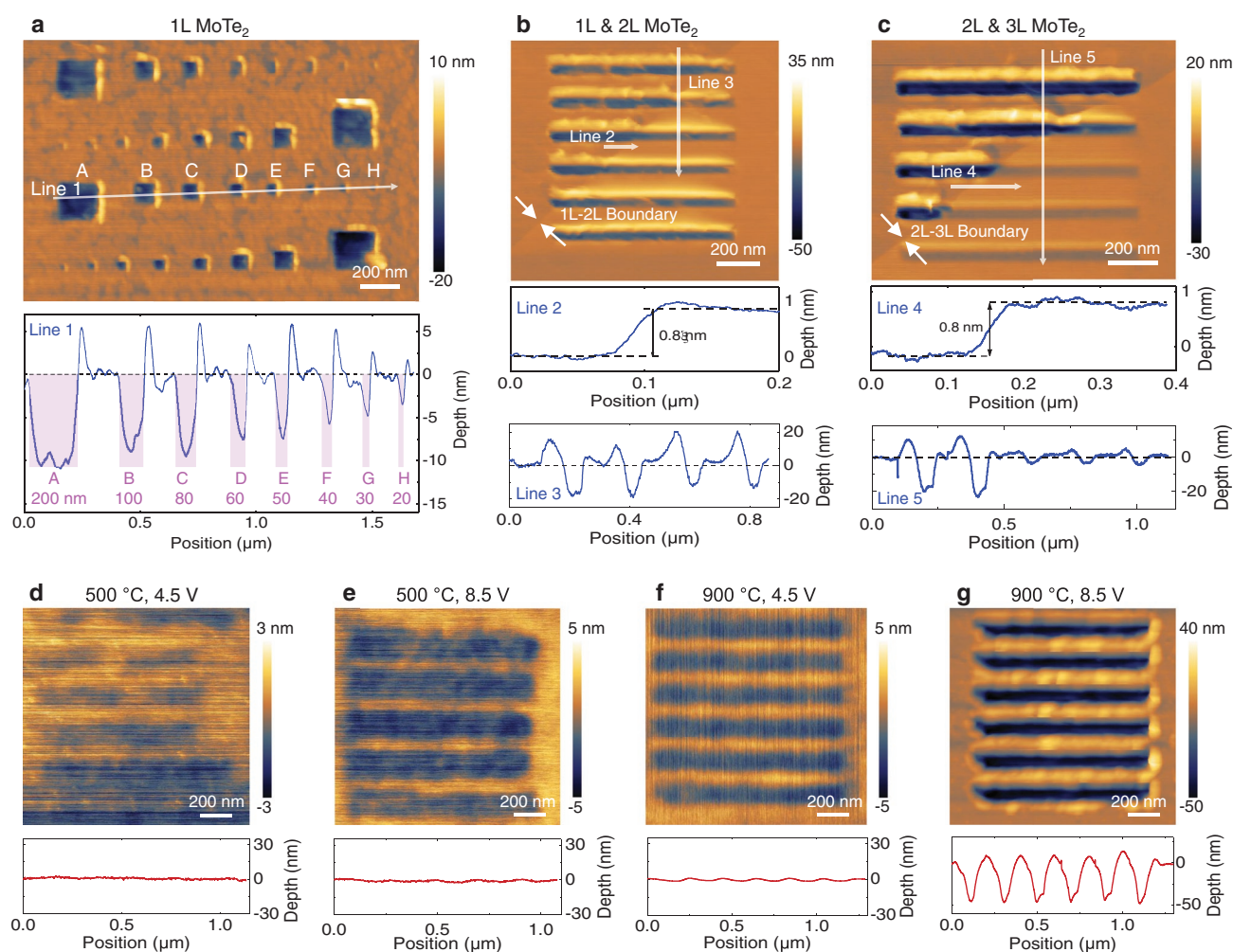


Figure 2. Versatility of the t-SPL nanocutting technique. a) AFM topography of nanosquare arrays in 1L MoTe₂ with feature sizes in the range from 20 to 200 nm and corresponding profile (Line 1). b) AFM topography of 1L and 2L MoTe₂ nanoribbon array with a linewidth of 50 nm (above) and the profiles corresponding to 1L–2L boundary (Line 2) and the selected cut area (Line 3) (below). c) AFM topography of 2L and 3L MoTe₂ nanoribbon array with a linewidth of 70 nm (above) and the profiles of 2L–3L boundary (Line 4) and a selected patterned area (Line 5) (below). d–g) Evaluation of effects of indentation voltage and temperature on the nanostructure generation on the same 1L MoTe₂: d) 500 °C and 4.5 V; e) 500 °C and 8.5 V; f) 900 °C and 4.5 V, and g) 900 °C and 8.5 V. The indicated temperature refers to the heater temperature. The temperature of the tip is a monotonic function of the heater temperature but difficult to estimate accurately.

failure strain of about 10% for MoTe₂,^[25] 10% for MoS₂,^[26] 2.6% for MoSe₂,^[27] and 12% for graphene,^[28,29] respectively, as confirmed by our experiments. For instance, a 1L MoS₂ concentric nanostructure and a 1L MoSe₂ nanoribbon array are also readily fabricated (Section S3, Supporting Information). Besides these, 1L MoS₂/1L MoTe₂ heterostructures were successfully cut with the highest indentation force that the used t-SPL system can provide. On the contrary, and as expected, graphene, even at monolayer thickness, cannot be fractured as the intra-layer bonding exceeds the force that can be applied with the t-SPL tool.^[28,29] This could be eventually overcome with a t-SPL cantilever that can apply larger contact forces. In addition, under the same parameters described in Figure 2g, we performed the nanocutting experiments on poly(methyl methacrylate) (PMMA). Unlike in the case of PPA the PMMA as supporting polymer layer does not sublime but only softens. By means of the probe indentation the 2D film is thereby locally strained but not cut (Section S4, Supporting Information).

The TMDCs with lower bond strength than graphene such as monolayer and bilayer MoTe₂ flakes have been readily cut (Figure 2b) into nanoribbon array. As expected, increasing the number of layers renders the cutting increasingly difficult, or impossible. For instance, the out-of-plane deformation of a 3L MoTe₂ flake is only about 4 nm, which is less than the breaking limit (Figure 2c). Again, this could be overcome by a t-SPL system with a higher indentation force. To further elucidate the detailed and combined effect of the tip-induced indentation force and the tip temperature, we wrote a series of patterns in a 1L MoTe₂ flake (Figure 2d–g) varying both values. The indentation force is $F_{in} = F_{el} - k_{ca}z_{offset} = k_{ca}(\Delta z - z_{offset})$, where F_{el} is the electrostatic force between the cantilever and the 2D layer, k_{ca} is the spring constant of the cantilever, z_{offset} is the height offset of the cantilever, and Δz is the deflection of the cantilever due to the combined effect of heating (bimorph effect) and applied voltage (electrostatic force).^[24] Figure 2d shows the topography of the patterned 2D layer at 500 °C and 4.5 V. In these conditions, the 2D layer is not broken and the PPA layer underneath cannot sublime. When the voltage is increased to 8.5 V, the 2D layer deforms downward out of plane by 5 nm for 70 nm wide patterns (Figure 2e). When the temperature is increased to 900 °C at 4.5 V, a similar out-of-plane strain occurs, which does not reach the failure strain (Figure 2f). Successful cutting of the 2D layer is achieved when the indentation voltage and the temperature are respectively increased to 8.5 V and 900 °C, (Figure 2g). This experiment demonstrates that high indentation force and high temperature are concurrently necessary to cleave the chemical bonds of the 2D material. During the cutting, the temperature at the 2D layer is less than the heater but over 150 °C, the sublimation temperature of PPA, as discussed previously.^[30,31] In the experiments performed here, the indentation force was estimated to be up to ≈310 nN for a heater temperature of 900 °C and an electrostatic potential between cantilever and substrate of 8.5 V, as further discussed in Section S5 in the Supporting Information. To determine the pressure exerted on the 2D material during the process, one has to take into account the contact area. If we assume a tip diameter of 30 ± 20 nm we obtain a pressure up to about 3.9 GPa, which is in the order of the required pressure for cutting 2D materials as listed in Table S1 Section S3 in the Supporting Information.

To characterize the physical properties of the 2D material nanostructures before and after the t-SPL cutting, we compare the Raman spectra of the nanostructured MoTe₂ flake patterned under different parameters. Figure 3a shows the three Raman spectra of the pristine, edge and cut areas, respectively. The Raman spectra of the edge area has the same peak positions at around 169 and 235 cm⁻¹ as the pristine area, but with 1/3 less intensity as expected from the ratio of patterned and pristine area within the observation spot (Figure 3b,c). The discriminative Raman peaks of MoTe₂ disappear after cutting, indicating the complete removal of the 2D material. Figure 3d shows the Raman spectra of a 1L MoTe₂ flake patterned at different indentation voltages. There is no peak position shift between the pristine material and the nanoribbon array, while there is a small but noticeable shift of 0.4 cm⁻¹ between pristine and strained area. This indicates that an indentation-induced strain is generated in the 2D material already at the low indentation force and no oxidation of MoTe₂ was observed as analyzed in wide-range Raman spectra (Section S6, Supporting Information). The Raman mapping of a MoTe₂ hexagonal microstructure (Figure 3g) shows that the intensities of the A_{1g}- (Figure 3h) and E_{2g}-band (Figure 3i) signals are clearly different in the cut areas (blue regions), edge areas (white regions), and pristine areas (red regions), further confirming the successful removal of the 2D material.

In the following, we describe the fabrication of two test devices to observe the evolution of the electrical resistance when the 2D material is progressively cut (Figure 4 and Section S7, Supporting Information). First, a 30 nm thick PPA layer is spin coated on a SiO₂/Si substrate with prefabricated 30 nm thick Au microelectrodes as shown in Figure 4b. Then, the laser direct-write head (a recently added feature of the NanoFrazor instrument) is used to remove the PPA polymer from the top of the electrodes (Figure 4c). A 1L MoTe₂ flake is dry transferred on this area resulting in electrical contact with the electrodes (Figure 4d). The t-SPL is then used to cut the 2D material at nanoscale as described earlier (Figure 4e). A schematic of the 2D material nanocutting is shown in Figure 4f. Figure 4g,h presents optical stereomicroscopy images of the devices corresponding to the step in Figure 4d, including the Au electrodes without PPA on top and the 1L MoTe₂ across the electrodes (colors have been enhanced for better visualization). Two-terminal resistive tracks have been created by successively cutting the side bands away to decrease the width of the conduction paths. Figure 4i presents topographies of the 2D layer on the substrate respectively before cutting and successively after the 1st, 2nd, 3rd, and final separation cut. This operation was performed under N₂ atmosphere to avoid oxidation. In order to demonstrate the capability of creating “sharp” cuts in 2D materials, *I*-*V* measurements were performed between each subsequent cut. The resistance of the conductive track increases from 25.4 GΩ for the uncut resistor up to infinite after the final cut, and scales accordingly with the dimension changes (Section S8, Supporting Information). Figure 4j shows the measured sheet resistance as a function of the channel width at the pristine condition and after the 1st, 2nd, 3rd, and final separation cut. As expected, the change in measured sheet resistance for the pristine and patterned flakes is negligible (a 6.7% maximum difference between the narrower microribbons and

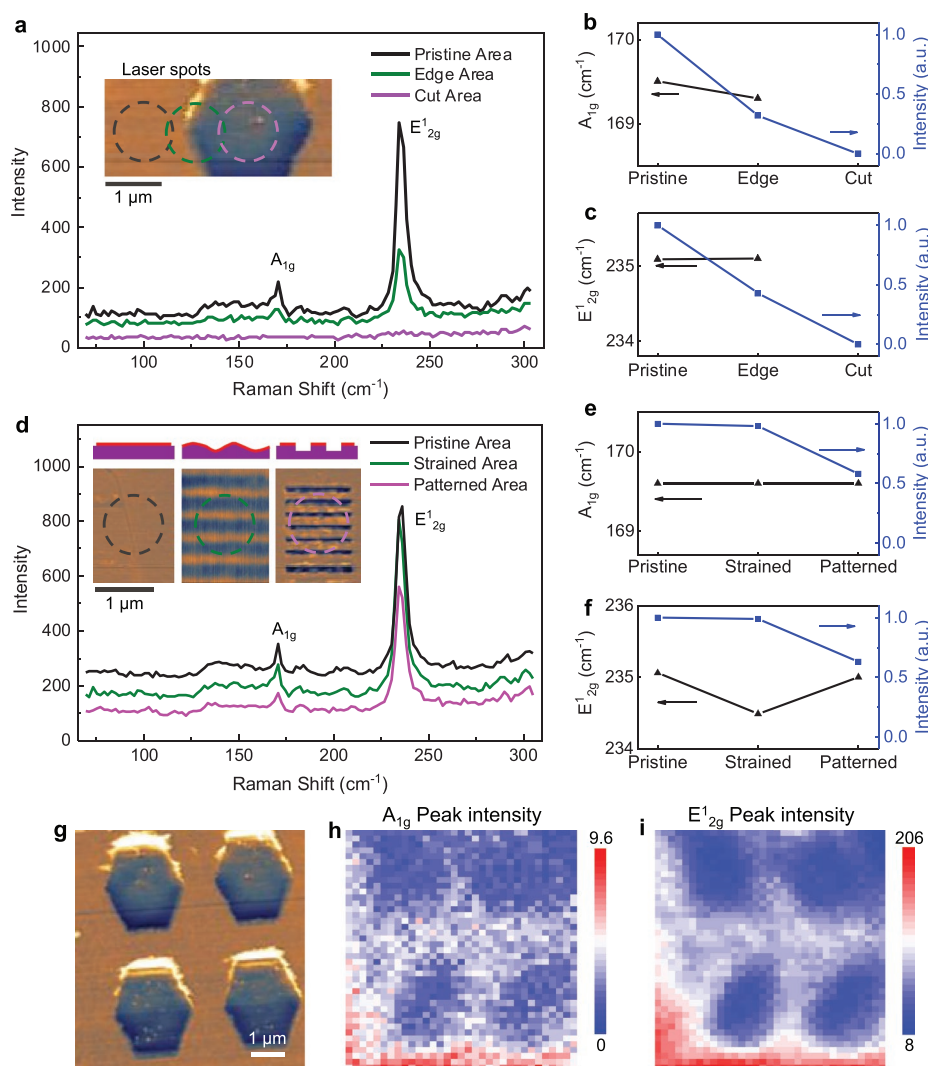


Figure 3. Raman spectra of 1L MoTe₂ micro/nanostructures fabricated using t-SPL. a) Raman signals for MoTe₂ at different regions. The insets show AFM topography of the structures for measurement. b) A_{1g} and c) E_{12g} peak positions and intensities in MoTe₂ for pristine, edge, and cut areas. d) Raman signals for MoTe₂ nanopatterns fabricated using different indentation force. The insets show AFM topographies for measurement. e) A_{1g} and f) E_{12g} peak positions and intensities in MoTe₂ with different indentation forces. g) AFM topography of MoTe₂ hexagonal microstructures. h,i) Raman intensity mapping of A_{1g} band (169 cm⁻¹) and E_{12g} band (235 cm⁻¹), respectively. The circles in (a) and (d) indicate the regions illuminated with the laser of the Raman spectroscopy.

the pristine 2D material is observed). Furthermore, cutting of a 200 nm wide nanoribbon array is demonstrated under the same condition as shown in Figure 4k. The measured sheet resistance of the monolayer nanoribbon array is also independent of the number of the nanoribbons (Figure 4l), and has a value comparable to that measured on SiO₂^[32] and about one order of magnitude larger than that measured on dangling-bond-free hexagonal boron nitride (h-BN).^[33] Such an increase in measured sheet resistance has been reported previously and it is presumably due to the trapped electronic states between the 2D material and the PPA polymer that modulate the conductivity.^[34] A possible solution to reduce the effect of PPA on the sheet resistance of the 2D material is to engineer the interface by adding an ultrathin dangling-bond-free material such as a monolayer or a few layers of h-BN between the PPA and the 2D film.^[35–39] Depending of the mechanical properties and

thickness of separating layer, the cutting might not be possible with the maximum indentation force of the specific commercial t-SPL cantilever used in this work, but it is within the reach of dedicated t-SPL cantilevers with larger spring constants.

Herein, we have demonstrated a high-resolution one-step nanolithography process for the direct nanocutting of 2D materials. Our approach is based on the use of a nanoscale hot tip that induces the rapid sublimation or plastic deformation of a polymeric layer and results in the breaking or stretching of the supported 2D materials. We demonstrated the cutting of monolayer MoTe₂, MoS₂, and MoSe₂ into various geometries including nanoribbons, nanosquares, and other arbitrary test patterns with resolution down to about 20 nm. This direct nanocutting process has potential applications in tailoring nanostructures of 2D materials for micro/nanoscale devices by a clean, one-step thermomechanical technique.

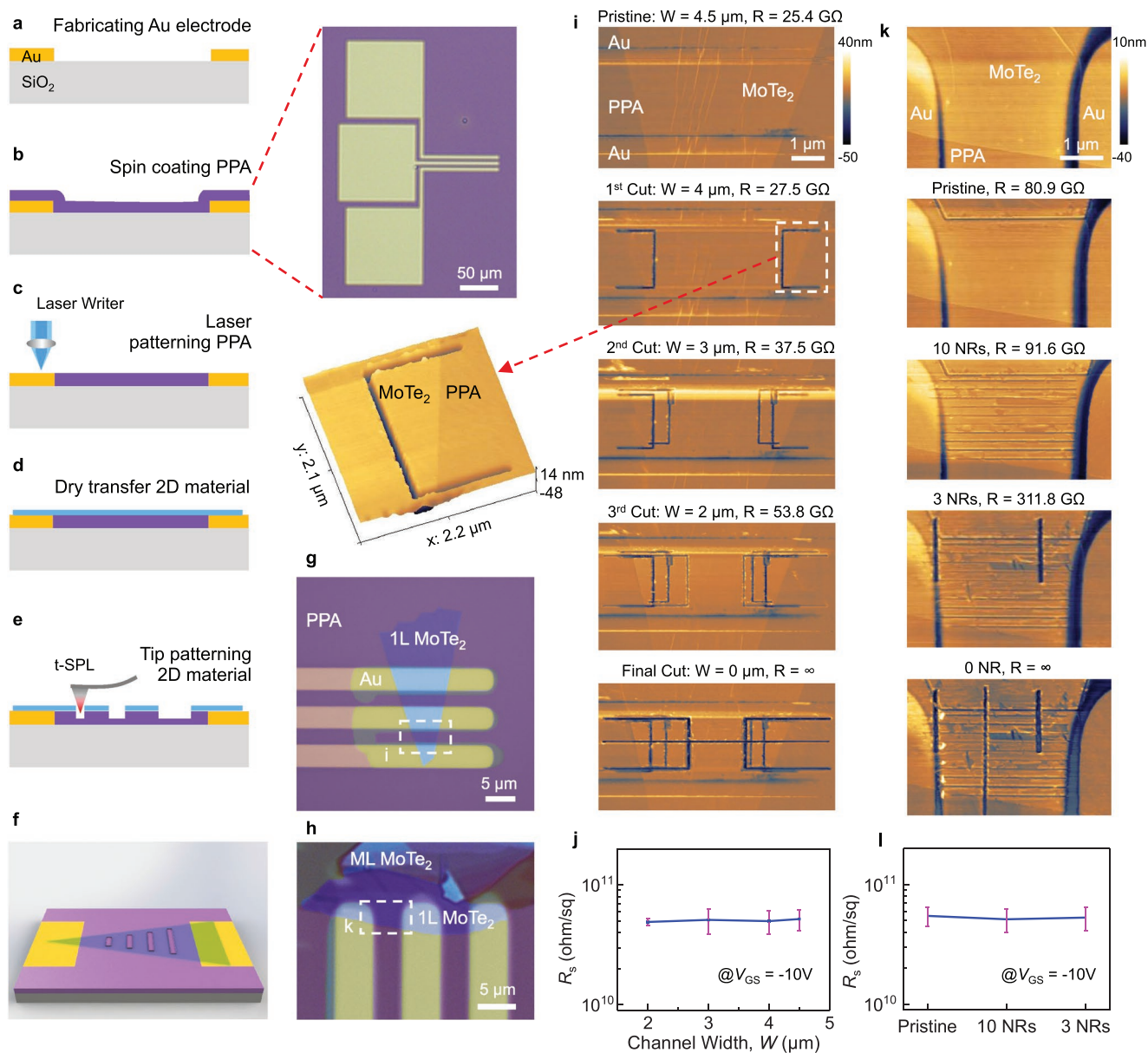


Figure 4. Nanocutting process of MoTe₂ micro/nanoribbon devices and their electrical characterization. a) Fabrication of Au microelectrodes on the SiO₂ substrate by standard photolithography. b) PPA layer is spin coated on top of the substrate. The inset is the optical stereomicroscopy image of the device with PPA. c) Direct laser removal of the PPA on top of Au electrodes. d) Dry transfer of the 2D material. e) The 2D layer is cut by the hot tip of the t-SPL and the PPA polymer film partially sublimates when the 2D layer is broken. f) 3D scheme of the patterned 2D device. g,h) False-colored optical stereomicroscopy images of the devices used in (i) and (k), respectively. i) AFM topographies of the flake on the substrate and after the 1st, 2nd, 3rd, and final cutting processes. The highlighted is the 3D profile of the cutting track. j) Measured sheet resistances (R_s) of the microribbon flake at the pristine condition, after 1st, 2nd, 3rd, and final cut. k) AFM topographies of the device in (h), after separation from the bulk flake and after successive cutting processes. l) Corresponding measured sheet resistances of the nanoribbons in (k).

Experimental Section

Material Preparation: PPA (Allresist) solution (3 wt% in anisole) is spin coated on SiO₂ (200 nm thick)/Si (500 μ m thick) substrate (conditions: 100 rpm for 5 s and then 6000 rpm for 60 s). MoTe₂ flakes are exfoliated from 2H-MoTe₂ bulk crystal onto poly(dimethylsiloxane) substrates then are transferred on the PPA substrate. The MoS₂, MoSe₂, and graphene flakes are obtained and processed with the same procedure. MoTe₂, MoS₂, and graphene crystals are purchased from HQ Graphene. MoSe₂ crystal is purchased from 2D Semiconductor.

Nanostructure Cutting: Cutting 2D materials is performed using a commercial t-SPL (NanoFrazor, SwissLitho AG, Switzerland). The cantilever is made of n-doped silicon. The spring constant of the tip is around 0.9 N m⁻¹.^[24] During the writing process, the tip is heated to reach a temperature above 150 °C at the 2D/PPA surface. The NanoFrazor has also an integrated 405 nm laser which is used to remove PPA on areas larger than a few square micrometers at a much higher speed than the hot tip.

Material and Structure Characterizations: AFM is performed to collect the topographies of the nanostructured or nanostrained 2D

materials. AFM is also used to verify the thickness of the nanoflakes. Images are collected using Bruker's Dimension FastScan AFM system. The FastScan AFM scanner mode (contact mode) is used. Raman spectroscopy is performed to confirm the layer number of all the exfoliated MoTe₂ flakes and to characterize the properties of the fabricated nanostructures. Raman spectra are collected using a confocal Raman microscope system (inVia Qontor, Renishaw) coupled with an Olympus inverted optical microscope, and using a laser source with an excitation wavelength of 532 nm. The laser power (84 μ W) is adjusted to avoid sample damage. Raman spectra are acquired in the range from 0 to 1800 cm⁻¹ with a 30 s exposure time and an average of three measurements. The peak at 520.7 cm⁻¹ from the silicon substrate is used as a reference.

Supporting Information

Supporting Information is available from the Wiley Online Library or from the author.

Acknowledgements

The authors thank the Center of Micro/Nanotechnology (CMi) of EPFL for the AFM facility support. This work has received funding from the European Research Council (ERC) under the European Union's Horizon 2020 research and innovation program (Project "MEMS 4.0," ERC-2016-ADG, Grant Agreement No. 742685).

Conflict of Interest

The authors declare no conflict of interest.

Keywords

2D materials, micro/nanoribbons, nanocutting, thermal scanning probe lithography, transition metal dichalcogenides

Received: February 21, 2020

Revised: April 11, 2020

Published online: June 11, 2020

- [1] B. Radisavljevic, A. Radenovic, J. Brivio, V. Giacometti, A. Kis, *Nat. Nanotechnol.* **2011**, 6, 147.
- [2] M. Chhowalla, D. Jena, H. Zhang, *Nat. Rev. Mater.* **2016**, 1, 16052.
- [3] N. Mounet, M. Gibertini, P. Schwaller, D. Campi, A. Merkys, A. Marrazzo, T. Sohier, I. E. Castelli, A. Cepellotti, G. Pizzi, N. Marzari, *Nat. Nanotechnol.* **2018**, 13, 246.
- [4] J. P. Llinas, A. Fairbrother, G. Borin Barin, W. Shi, K. Lee, S. Wu, B. Yong Choi, R. Braganza, J. Lear, N. Kau, W. Choi, C. Chen, Z. Pedramrazi, T. Dumslaff, A. Narita, X. Feng, K. Müllen, F. Fischer, A. Zettl, P. Ruffieux, E. Yablonovitch, M. Crommie, R. Fasel, J. Bokor, *Nat. Commun.* **2017**, 8, 633.
- [5] S. Chen, S. Kim, W. Chen, J. Yuan, R. Bashir, J. Lou, A. M. van der Zande, W. P. King, *Nano Lett.* **2019**, 19, 2092.
- [6] A. Dathbun, Y. Kim, Y. Choi, J. Sun, S. Kim, B. Kang, M. S. Kang, D. K. Hwang, S. Lee, C. Lee, J. H. Cho, *ACS Appl. Mater. Interfaces* **2019**, 11, 18571.
- [7] Y. Ye, L. Gan, L. Dai, Y. Dai, X. Guo, H. Meng, B. Yu, Z. Shi, K. Shang, G. Qin, *Nanoscale* **2011**, 3, 1477.
- [8] D. S. Fox, Y. Zhou, P. Maguire, A. O'Neill, C. O'Coileáin, R. Gatensby, A. M. Glushenkov, T. Tao, G. S. Duesberg, I. V. Shvets, M. Abid, M. Abid, H.-C. Wu, Y. Chen, J. N. Coleman, J. F. Donegan, H. Zhang, *Nano Lett.* **2015**, 15, 5307.
- [9] J. C. Meyer, F. Eder, S. Kurasch, V. Skakalova, J. Kotakoski, H. J. Park, S. Roth, A. Chuvilin, S. Eychen, G. Benner, A. V. Krashenninnikov, U. Kaiser, *Phys. Rev. Lett.* **2012**, 108, 196102.
- [10] B. J. Lee, B. J. Lee, J. Lee, J.-W. Yang, K.-H. Kwon, *Thin Solid Films* **2017**, 637, 32.
- [11] L. Lin, J. Li, W. Li, M. N. Yogeesh, J. Shi, X. Peng, Y. Liu, B. B. Rajeeva, M. F. Becker, Y. Liu, D. Akinwande, Y. Zheng, *Adv. Funct. Mater.* **2018**, 28, 1803990.
- [12] J. B. Park, J.-H. Yoo, C. P. Grigoropoulos, *Appl. Phys. Lett.* **2012**, 101, 043110.
- [13] Y. Wu, H. Tao, S. Su, H. Yue, H. Li, Z. Zhang, Z. Ni, X. Chen, *Sci. Rep.* **2017**, 7, 46583.
- [14] Q. Yu, L. A. Jauregui, W. Wu, R. Colby, J. Tian, Z. Su, H. Cao, Z. Liu, D. Pandey, D. Wei, T. F. Chung, P. Peng, N. P. Guisinger, E. A. Stach, J. Bao, S.-S. Pei, Y. P. Chen, *Nat. Mater.* **2011**, 10, 443.
- [15] A. J. Way, R. M. Jacobberger, M. S. Arnold, *Nano Lett.* **2018**, 18, 898.
- [16] R. Garcia, A. W. Knoll, E. Riedo, *Nat. Nanotechnol.* **2014**, 9, 577.
- [17] G. Lu, X. Zhou, H. Li, Z. Yin, B. Li, L. Huang, F. Boey, H. Zhang, *Langmuir* **2010**, 26, 6164.
- [18] Y. K. Ryu, R. Garcia, *Nanotechnology* **2017**, 28, 142003.
- [19] Z. Wei, D. Wang, S. Kim, S.-Y. Kim, Y. Hu, M. K. Yakes, A. R. Laracuate, Z. Dai, S. R. Marder, C. Berger, W. P. King, W. A. de Heer, P. E. Sheehan, E. Riedo, *Science* **2010**, 328, 1373.
- [20] A. W. Knoll, D. Pires, O. Coulembier, P. Dubois, J. L. Hedrick, J. Frommer, U. Duerig, *Adv. Mater.* **2010**, 22, 3361.
- [21] S. Howell, A. Grushina, F. Holzner, J. Brugger, *Microsyst. Nanoeng.* **2020**, 6, 21.
- [22] X. Zheng, A. Calò, E. Albisetti, X. Liu, A. S. M. Alharbi, G. Arefe, X. Liu, M. Spieser, W. J. Yoo, T. Taniguchi, K. Watanabe, C. Aruta, A. Ciarrocchi, A. Kis, B. S. Lee, M. Lipson, J. Hone, D. Shahrjerdi, E. Riedo, *Nat. Electron.* **2019**, 2, 17.
- [23] O. Coulembier, A. Knoll, D. Pires, B. Gotsmann, U. Duerig, J. Frommer, R. D. Miller, P. Dubois, J. L. Hedrick, *Macromolecules* **2010**, 43, 572.
- [24] F. Holzner, *Thermal Scanning Probe Lithography Using Polyphthalaldehyde*, Ph.D. Thesis, ETH Zürich, Zürich (Switzerland), DISS ETH, Nr. 20962 **2013**, <https://doi.org/10.3929/ethz-a-009756918>.
- [25] Y. Sun, J. Pan, Z. Zhang, K. Zhang, J. Liang, W. Wang, Z. Yuan, Y. Hao, B. Wang, J. Wang, Y. Wu, J. Zheng, L. Jiao, S. Zhou, K. Liu, C. Cheng, W. Duan, Y. Xu, Q. Yan, K. Liu, *Nano Lett.* **2019**, 19, 761.
- [26] S. Bertolazzi, J. Brivio, A. Kis, *ACS Nano* **2011**, 5, 9703.
- [27] Y. Yang, X. Li, M. Wen, E. Hacıopian, W. Chen, Y. Gong, J. Zhang, B. Li, W. Zhou, P. M. Ajayan, Q. Chen, T. Zhu, J. Lou, *Adv. Mater.* **2017**, 29, 1604201.
- [28] C. Lee, X. Wei, J. W. Kysar, J. Hone, *Science* **2008**, 321, 385.
- [29] C. Lee, X. Wei, Q. Li, R. Carpick, J. W. Kysar, J. Hone, *Phys. Status Solidi* **2009**, 246, 2562.
- [30] B. Gotsmann, M. A. Lantz, A. Knoll, U. Dürig, in *Nanotechnology*, Wiley-VCH Verlag GmbH & Co. KGaA, Weinheim, Germany **2010**.
- [31] B. Nelson, W. King, *Nanoscale Microscale Thermophys. Eng.* **2008**, 12, 98.
- [32] W. Luo, M. Zhu, G. Peng, X. Zheng, F. Miao, S. Bai, X.-A. Zhang, S. Qin, *Adv. Funct. Mater.* **2018**, 28, 1704539.
- [33] S. Larentis, B. Fallahazad, H. C. P. Movva, K. Kim, A. Rai, T. Taniguchi, K. Watanabe, S. K. Banerjee, E. Tutuc, *ACS Nano* **2017**, 11, 4832.

- [34] I. Amit, T. J. Octon, N. J. Townsend, F. Reale, C. D. Wright, C. Mattevi, M. F. Craciun, S. Russo, *Adv. Mater.* **2017**, *29*, 1605598.
- [35] D. Unuchek, A. Ciarrocchi, A. Avsar, Z. Sun, K. Watanabe, T. Taniguchi, A. Kis, *Nat. Nanotechnol.* **2019**, *14*, 1104.
- [36] A. Avsar, K. Marinov, E. G. Marin, G. Iannaccone, K. Watanabe, T. Taniguchi, G. Fiori, A. Kis, *Adv. Mater.* **2018**, *30*, 1707200.
- [37] L. Wang, B. Wu, J. Chen, H. Liu, P. Hu, Y. Liu, *Adv. Mater.* **2014**, *26*, 1559.
- [38] J. Lee, T.-J. Ha, K. N. Parrish, S. F. Chowdhury, L. Tao, A. Dodabalapur, D. Akinwande, *IEEE Electron Device Lett.* **2013**, *34*, 172.
- [39] L. H. Li, E. J. G. Santos, T. Xing, E. Cappelluti, R. Roldán, Y. Chen, K. Watanabe, T. Taniguchi, *Nano Lett.* **2015**, *15*, 218.